

See discussions, stats, and author profiles for this publication at: <https://www.researchgate.net/publication/261638598>

QM/MM Free-Energy Simulations of Reaction in *Serratia marcescens* Chitinase B Reveal the Protonation State of Asp142 and the Critical Role of Tyr214

ARTICLE *in* THE JOURNAL OF PHYSICAL CHEMISTRY B · APRIL 2014

Impact Factor: 3.3 · DOI: 10.1021/jp500652x · Source: PubMed

CITATIONS

3

READS

48

3 AUTHORS, INCLUDING:



Jitrayut Jitonnom

University of Phayao

15 PUBLICATIONS 67 CITATIONS

[SEE PROFILE](#)



Michael Limb

University of Bristol

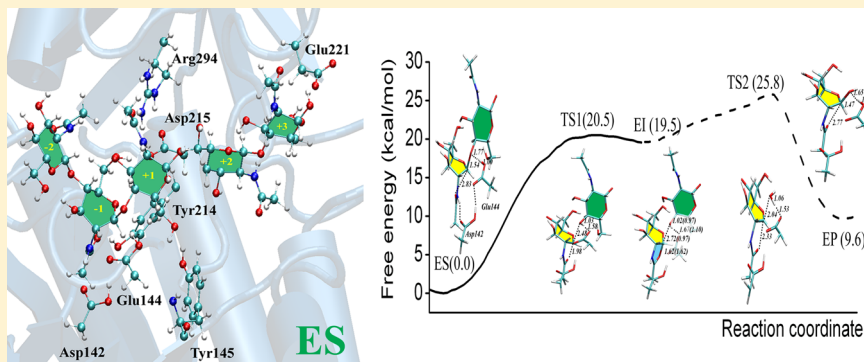
2 PUBLICATIONS 5 CITATIONS

[SEE PROFILE](#)

QM/MM Free-Energy Simulations of Reaction in *Serratia marcescens* Chitinase B Reveal the Protonation State of Asp142 and the Critical Role of Tyr214

Jitrayut Jitonnom,^{*,†} Michael A. L. Limb,[‡] and Adrian J. Mulholland[‡][†]Division of Chemistry, School of Science, University of Phayao, Phayao 56000, Thailand[‡]Centre for Computational Chemistry, School of Chemistry, University of Bristol, Bristol BS8 1TS, U.K.

Supporting Information



ABSTRACT: *Serratia marcescens* Chitinase B (ChiB), belonging to the glycosidase family 18 (GH18), catalyzes the hydrolysis of β -1,4-glycosidic bond, with retention of configuration, via an unusual substrate-assisted mechanism, in which the substrate itself acts as an intramolecular nucleophile. Here, both elementary steps (glycosylation and deglycosylation) of the ChiB-catalyzed reaction are investigated by means of combined quantum mechanics/molecular mechanics (QM/MM) umbrella sampling molecular dynamics (MD) simulations at the SCC-DFTB/CHARMM22 level of theory. We examine the influence of the Asp142 protonation state on the reaction and the role that this residue performs in the reaction. Our simulations show that reaction with a neutral Asp142 is preferred and demonstrate that this residue provides electrostatic stabilization of the oxazolinium ion intermediate formed in the reaction. Insight into the conformational itinerary ($^{14}\text{B} \leftrightarrow ^4\text{H}_5 \leftrightarrow ^4\text{C}_1$) adopted by the substrate (bound in subsite -1) along the preferred reaction pathway is also provided by the simulations. The relative energies of the stationary points found along the reaction pathway calculated with SCC-DFTB and B3LYP were compared. The results suggest that SCC-DFTB is an accurate method for estimating the relative barriers for both steps of the reaction; however, it was found to overestimate the relative energy of an intermediate formed in the reaction when compared with the higher level of theory. Glycosylation is suggested to be a rate-determining step in the reaction with calculated overall reaction free-energy barrier of 20.5 kcal/mol, in a reasonable agreement with the 16.1 kcal/mol barrier derived from the experiment. The role of Tyr214 in catalysis was also investigated with the results, indicating that the residue plays a critical role in the deglycosylation step of the reaction. Simulations of the enzyme–product complex were also performed with an unbinding event suggested to have been observed, affording potential new mechanistic insight into the release of the product of ChiB.

INTRODUCTION

Glycoside hydrolases, or glycosidases (GHS), are the largest group of glycan-degrading enzymes in nature. They are responsible for hydrolysis of glycosidic bonds in carbohydrates and help to catalyze a wide range of important biological functions, such as glycan processing in glycoproteins, remodeling cell walls, and polysaccharide modification and degradation.¹ In addition to their numerous roles in biochemistry, they are highly efficient enzymes, accelerating reactions by as much as 10^{17} times over the spontaneous rate.²

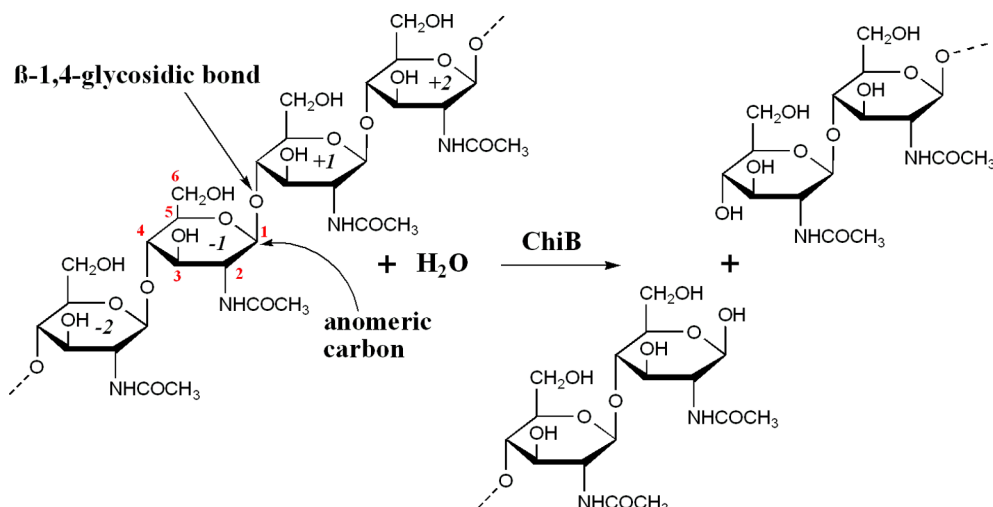
GHS have been extensively studied, with >130 different families of GHS reported in the literature;³ however, despite

advances in understanding of the mechanisms underlying GH catalysis, the specific mechanistic details of many GHS remain an important challenge. The first general mechanism for GHS was proposed by Koshland⁴ in late 1953: he suggested an acid–base type catalysis, which could proceed with either a retention or an inversion of the anomeric configuration of the substrate. In the ensuing years, a wealth of research (extensively reviewed elsewhere^{5,6}) has provided a more detailed description of GH

Received: January 20, 2014

Revised: April 14, 2014

Published: April 15, 2014

Scheme 1. General Representation of the Substrate and Product of the ChiB-Catalyzed Hydrolysis^a

^aChiB catalyzes the cleavage of the β -1,4-glycosidic bond between the NAG residues in subsites -1 and $+1$ of chitin, a polysaccharide (4 units shown) consisting of *N*-acetylglucosamine (GlcNAc or NAG) units linked by β -1,4-glycosidic bonds.

function. In brief, inverting GHs operate by a single nucleophilic substitution with only one transition state, whereas retaining GHs follow a double displacement mechanism, proceeding via a stable covalent glycosyl–enzyme intermediate (glycosylation step), followed by the subsequent hydrolysis of this intermediate to form the cleaved reaction product (deglycosylation step). Inverting and retaining GHs usually require the presence of at least two key residues in the active site of the enzyme, one acting as the general acid and the other as the general base, in order for efficient catalysis to take place. In some GHs, however, suitable residues required to perform these specific roles are absent from, or poorly positioned, within the enzyme active site and therefore cannot contribute to catalysis in this proposed manner. This has led to an alternative mechanism, known as the substrate-assisted mechanism, to be proposed for these types of GHs.

Glycosidic bond hydrolysis occurring via a substrate-assisted catalytic mechanism is an unusual case observed in some glycosidases, where the substrate itself acts as an intramolecular nucleophile instead of an enzyme residue.⁷ This mechanism is thought to be used by some retaining GHs enzymes (families 18, 20, 56, 84, and 85) acting on substrates containing an *N*-acetyl (acetamido) group at the C2 position, several GH3 and GH22 enzymes,^{8,9} and inverting GH19 enzymes.¹⁰ Additionally, participation of the *N*-acetyl group has also been proposed to take place in glycosyltransferase.¹¹ It is believed that all these enzymes share a common mechanistic feature, where in the absence of a suitably positioned nucleophilic residue in the enzyme active site, the acetamido group on the substrate is instead directly involved in the formation of the intermediate (proposed to be either an oxazoline or oxazolinium) in the first step of the reaction.⁷ Several crystal structures of GH18, GH20, GH56, GH84, and GH85 family enzymes have been solved, and in conjunction with several experimental^{12–15} and computational investigations,^{7,16,17} the substrate-assisted mechanism is suggested to be an accurate description of the enzyme-catalyzed reaction in these enzymes.

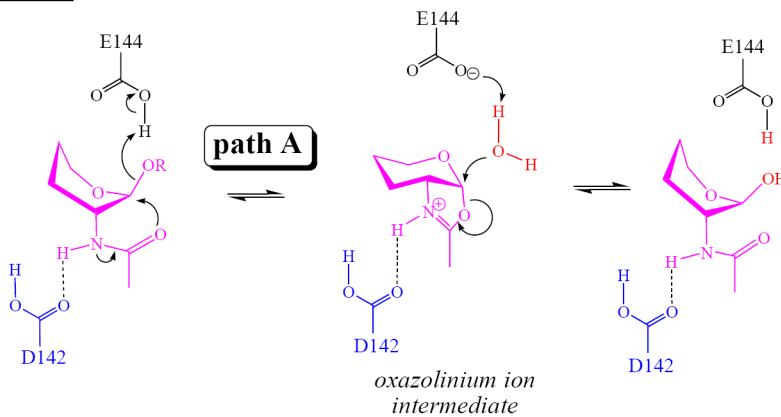
S. marcescens Chitinase B (ChiB), belonging to the GH18 family, degrades chitin [an insoluble linear polymer of β -(1,4)-linked *N*-acetylglucosamine (NAG)_n], which is the second-most abundant biopolymer in nature after cellulose. ChiB has

received much attention as an attractive system for the development of new inhibitors with chemotherapeutic potential.^{18,19} It has also been applied in biotechnology for conversion of insoluble polysaccharides into a commercially valuable product.²⁰ It is proposed that ChiB catalyzes the hydrolysis of the glycosidic bonds found in chitin via the aforementioned substrate-assisted mechanism (see Scheme 1). Previous studies on ChiB have indicated that the enzyme's catalytic function depends on a relatively large number of residues:²¹ Glu144 is proposed to act as a catalytic acid/base,¹⁵ Asp142 and Asp140 are suggested to be involved in the binding of substrates as well as catalysis,²¹ and a variety of other conserved residues (e.g., Tyr10, Ser93, Tyr214, and Asp215) have also been found to influence the catalytic activity of the enzyme.²¹ Of these residues, Asp142 and Tyr214 are of particular interest because their mechanistic roles are still not fully understood.

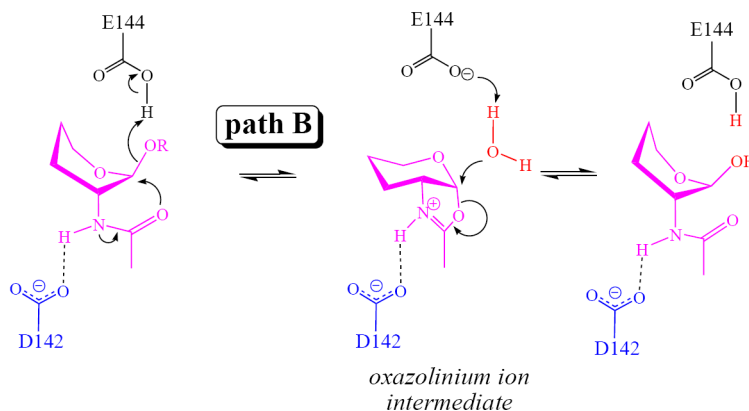
In our recent theoretical study, we modeled the glycosylation reaction of ChiB using QM/MM potential energy surface calculations, treating the Asp142 as a neutral residue.⁷ Our calculations suggested that Asp142, when in its neutral form, plays a critical role in catalysis by electrostatically stabilizing the transition state and oxazolinium ion intermediate formed in the glycosylation step of the reaction. The study provided useful insight into the preferred catalytic pathway for the reaction when the Asp142 is treated as a protonated residue. However, when comparing the protonation state of the Asp142 residue in ChiB to its analogous residue in a variety of similar GHs (Asp313 in *Streptomyces plicatus* hexosaminidase, GH20,²² and Asp174 in human O-GlcNAcase, GH84),²³ all of which proceed via a substrate-assisted mechanism, it is found that these similar enzymes follow a reaction mechanism where the deprotonated form of the residue is favored. Consequently, it is still not fully understood why the protonated form of the Asp142 residue is preferred in ChiB and what the fundamental impact this difference has on the role of the residue in the reaction. Therefore, in order to investigate the origin of this preference for the neutral protonation state of this vital active site residue, both possible protonation states of the residue were modeled, by simulating three possible reaction pathways for the ChiB-catalyzed reaction (Scheme 2).

Scheme 2. (A–C) Three Reaction Pathways for Hydrolysis of Chitin by ChiB Modeled in This Study Utilizing QM/MM Umbrella Sampling MD

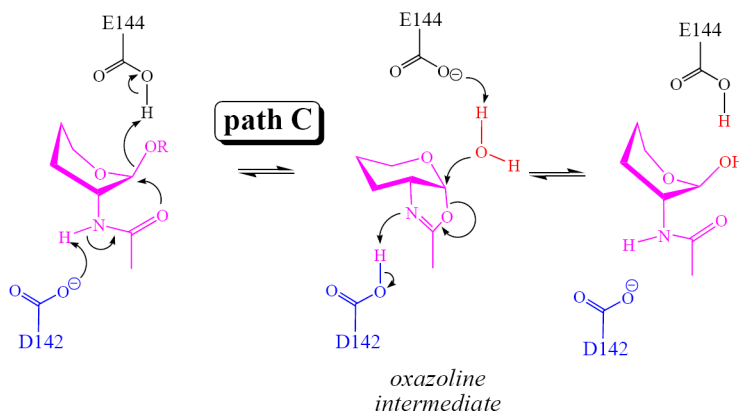
neutral Asp142



ionized Asp142



path C



Tyr214, in conjunction with Asp142 and Asp215, is proposed to interact with the substrate upon binding. Specifically, Tyr214 has been observed in the crystal structure to form an interaction which contributes to the distortion of the *N*-acetyl group on the -1 sugar.^{15,21} Despite the presence of this apparently favorable interaction with the substrate, mutagenesis study²¹ has shown that k_{cat} , and not K_m , is affected by the Y214F mutation ($0.117 \pm 0.011 \text{ s}^{-1}$), resulting in a 160-fold decrease in the k_{cat} compared with the wild-type ($17.8 \pm 2.3 \text{ s}^{-1}$) at pH 6.3. Similar perturbations to the rate have also been observed in Y390F in ChiA,²⁴ Y183F in hevamine,²⁵ and Y227F in ChiNCTU2.²⁶ The reason for this significant reduction in the rate and also catalytic activity upon mutation

of Tyr214 remains largely unresolved. Currently it is proposed, based on evidence from experimental studies looking at the binding of reaction intermediate analogues^{27,28} and our recent theoretical study,⁷ that the Tyr214 plays an important role in destabilizing intermediates formed during the enzyme-catalyzed reaction and, hence, it is this that could account for the observed decrease in the k_{cat} upon mutation on the residue. In our computational study, the calculations concluded that destabilization of the oxazolinium ion intermediate is provided by a hydrogen bond formed between the Tyr214 hydroxyl group and the *N*-acetyl group of the -1 subsite NAG; however, any further insights into the role the residue plays in the later parts of the reaction was not obtained, as our calculations did

not include modeling of the deglycosylation step of the reaction. In this study, the catalytic role of the two conserved residues, Asp142 and Tyr214, was investigated by performing combined QM/MM (quantum mechanics/molecular mechanics) molecular dynamics (MD) simulations. Three different reaction pathways (see Scheme 2) were modeled to investigate the most likely protonation state of Asp142 residue in the reaction (neutral/protonated or ionized/deprotonated) and to provide a more detailed understanding of the catalytic mechanism of *S. marcescens* ChiB at the atomic level. Both the glycosylation and the deglycosylation steps of the reaction were modeled utilizing adiabatic mapping calculations.⁷ For the first time, the free energy for the complete catalytic reaction for the ChiB was calculated, in order to determine the most likely pathway of the full ChiB-catalyzed reaction. Higher level energy corrections (using hybrid density functional theory) were also performed on the structures obtained to validate the computational methods used for the reaction pathway calculations. The role of Tyr214 in catalysis was examined via hydrogen bond analysis, and free-energy calculations were utilized to assess the quantitative contribution of this residue to the calculated free-energy barrier of the reaction in ChiB.

■ COMPUTATIONAL DETAILS

The initial structure of the enzyme–substrate (ES) complex was taken from the X-ray structure of the E144Q mutant of *S. marcescens* ChiB with a chitopentaose substrate bound (PDB code 1E6N).¹⁵ The wild-type was recovered by manually altering Gln144 to Glu144. Two different models (neutral and negatively charged/ionized), differing in the protonation state of the catalytic residue Asp142, were prepared to test the proposed catalytic mechanisms (Scheme 2). These were generated from the wild-type structure using a standard patch in CHARMM to adjust the Asp142 protonation state. All crystallographic water molecules were retained. Hydrogen atoms were added using the HBUILD subroutine in CHARMM, and the titratable residues in the enzymes were assigned based on the pK_a estimated by PROPKA 2.0 (<http://propka.ki.ku.dk>)²⁹ at their physiological pH. The protonation state of the catalytic triad (Asp140-Asp142-Glu144) for the two models was different: in both, Asp140 was deprotonated and Glu144 was protonated, with Asp142 deprotonated in the ionized model but treated as protonated in the neutral model. All other aspartate and glutamate residues were treated as deprotonated. Histidine residues (none of which are located near the active site) were modeled in their neutral states, with their tautomeric state assigned on the basis of the hydrogen-bonding network using WHAT-IF (<http://swift.cmbi.ru.nl>).³⁰ All simulations were performed using the CHARMM program (version c27b2).³¹

For the QM/MM MD simulations, the system was partitioned into two regions: a QM region consisting of a relatively small number of atoms directly involved in the reaction and a MM region consisting of all the remaining atoms in the system in order to include the important long-range effect of protein/solvent environment in the calculation. The QM region (see Figure 2c) for the glycosylation step consisted of the side-chains of the Glu144 and Asp142 and the NAG residues at subsites -1 and +1 of the substrate (chitobiose), for a total of 72 and 73 atoms for ionized and neutral Asp142 model, respectively. The QM region for the deglycosylation step was different to the one used to model the first step of the reaction and consisted of the NAG monomer at subsite -1 of

the substrate (a chitose unit), the side-chains of Glu144 and Asp142, and a catalytic water molecule, for a total of 45 and 46 atoms for ionized and neutral Asp142 model, respectively. The selection of the catalytic water molecule for the deglycosylation step was based on the product of the preceding glycosylation step, where the water observed in the QM/MM MD simulations (Figure S1 of the Supporting Information) to be best positioned for nucleophilic attack was treated with QM methods. In addition, the aglycon leaving group at subsites +1, +2, and +3 was removed from the enzyme active site and replaced by TIP3P water molecules for the deglycosylation step. The QM regions were treated using a self-consistent charge-density functional tight-binding (SCC-DFTB) method³² as implemented in CHARMM.³³ SCC-DFTB has successfully been applied to study reactions in several important enzymes.^{34–36} The MM regions for both reaction steps, consisting of all the remaining enzyme, substrate, and solvent molecules not included in the QM region, were described with the CHARMM22 all-atom force field³⁷ and additional parameters for the NAG moieties, as used in our previous study.⁷ Hydrogen “QQ” type link-atoms³⁸ were placed along covalent bonds crossing the QM/MM boundary and were situated between the C_β and C_α atoms of the enzyme residues and along the C–O bond of the glycosidic linkage for both sugar moieties in the substrate (requiring 4 H-link atoms for the glycosylation step and 2 H-link atoms for the deglycosylation step).

The systems were prepared for QM/MM MD simulations using the same protocols applied successfully in our earlier study.⁷ In brief, the ES complex was solvated by a 25 Å radius sphere of pre-equilibrated TIP3P model waters^{37,39} centered on the anomeric C1 carbon (see Scheme 1). A spherical deformable boundary potential⁴⁰ with a 25 Å radius was used to prevent the water from “evaporating” from the system. All atoms outside the 25 Å sphere centered on the anomeric carbon were deleted, while protein heavy atoms in the buffer zone (21–25 Å) were subject to Langevin dynamics with positional restraints using force constants scaled to increase from the inside to the outside of the buffer. All atoms within a 21 Å sphere of the reaction zone were subjected to Newtonian dynamics with no positional restraints. The ES complex for each system was thermalized in the NVT ensemble at 310 K with 1 ns of stochastic boundary QM/MM MD simulation, following the procedure described in refs 7 and 41. An integration time-step of 1 fs was used, with all of the bonds involving hydrogen atoms constrained using SHAKE.⁴²

Several snapshots were taken from the equilibrated QM/MM MD simulations, 300–1000 ps, to ensure a diverse range of enzyme–substrate conformations were sampled, which has been found to be important in similar studies.^{7,43} These initial geometries, extracted from MD, were subsequently energy-minimized with the Adopted Basis Newton–Raphson method until the gradient was <0.01 kcal/(mol Å), to be used as starting points for QM/MM adiabatic mapping calculations.⁴⁴ For modeling of the reaction by adiabatic mapping, the reaction coordinates for both steps of the reaction (glycosylation and deglycosylation) along the paths A–C (Scheme 2) are linear combinations of interatomic distances as defined in Figure S2 of the Supporting Information. Potential energy surfaces (PESs) were calculated, and the geometries representing the minimum energy pathway (MEP) through the surfaces were used as the putative reaction coordinates for the free energy (potential of mean force, PMF) calculations.

The free-energy profile for each pathway was computed using QM/MM umbrella sampling MD simulations requiring a series of simulations to be performed with a harmonically restrained reaction coordinate utilizing a force constant of 200 kcal/(mol Å²). All other aspects of the umbrella sampling simulations were the same as the QM/MM MD simulations described above. Each simulation (window) consisted of 60 ps of equilibration and 40 ps of sampling dynamics. The free-energy profiles were obtained by combining the statistics from all of the simulations performed for each reaction using the weighted histogram analysis method (WHAM).⁴⁵ These approaches have been applied successfully in previous work for other enzymes,^{46,47} including the GH5 member Cel5A cellulase.³⁴

RESULTS AND DISCUSSION

QM/MM MD Simulations of Enzyme–Substrate Complex. Two 1 ns QM/MM MD simulations of the Michaelis complexes, with Asp142 treated as ionized and neutral, were conducted to obtain the initial average active-site structures for reaction modeling. The simulations indicate that both ES complexes stable, reaching the equilibrium after the first 300 ps of the simulations, as indicated by the root-mean-square deviations (RMSD) relative to the starting structure calculated for the simulations (Figure 1a). The ionized model (0.28 ± 0.01 Å) exhibits a slightly higher RMSD compared to the neutral model (0.24 ± 0.01 Å). Snapshots of the ES complex for both models are shown in Figure 2 (panels a and b). The substrate was found to bind within the enzyme active sites via a combination of hydrogen bonds (H-bonds) and van der Waals interactions for the majority of the simulation. These

interactions maintained the distortion of the pyranose ring in the -1 subsite in the boat conformation (see angles C2–C1–O5–C5 and C3–C2–C1–O5 in Table S1 of the Supporting Information), consistent with the experimentally determined crystal structure.¹⁵ Tyr214 and Asp142 both make major contributions to this distortion by forming tight H-bond interactions with the N-acetyl group of the -1 sugar ($d_6 = 1.93 \pm 0.13/1.68 \pm 0.08$ Å and $d_9 = 1.70 \pm 0.10/1.75 \pm 0.11$ Å for neutral/ionized models, respectively; Figure 2c and Table S1 of the Supporting Information), enabling the oxygen atom of the N-acetyl to move toward the anomeric carbon ($d_4 = 2.85 \pm 0.13/2.92 \pm 0.14$ Å for neutral/ionized models, respectively; Table S1 of the Supporting Information), thus helping to promote intramolecular nucleophilic attack by narrowing the distance between the two atoms. The other sugar subsites (-2 , $+2$, $+3$) remained in a chair conformation, stabilized by the solvent-exposed aromatic residues (e.g., Trp97 and Trp220) and, to a lesser extent, by hydrogen bonding. Interestingly, a loss of the H-bond interaction between Asp142 and Glu144 (see Figure 1b) was observed in some parts of the simulation in the ionized model; this meant the Glu144 side chain could move away from the Asp142 carboxyl group and point toward Tyr145 (Figure 2b). In this new position, the side chains of both Asp142 and Glu144 were now exposed to the solvent (Figure S3 of the Supporting Information), therefore preventing them from interacting effectively with substrate. Despite this observation in the ionized model simulations, the Glu144 residue on average, in both models, was found to be well-positioned for proton donation to the glycosidic bond, as required for the first step of the reaction, with a favorable d_2 distance of ~ 1.8 Å maintained over the course of both simulations.

Protonation State of Asp142 and Catalytic Mechanism of *S. marcescens* ChiB. Two carboxyl residues (Glu144 and Asp142) in ChiB are proposed to play a crucial role during hydrolysis; while Glu144 is known to function as a catalytic acid/base, the influence of the chosen protonation state of the Asp142 residue and its impact on the residue as an electrostatic stabilizer⁷ is still not fully understood. Here, three reaction pathways were modeled in order to determine which was the most likely description of the ChiB-catalyzed reaction and to investigate the effect of the protonation state of Asp142. The mechanistic details of the pathways modeled are shown in Scheme 2. In the first pathway (denoted as “path A”), the reaction proceeds via an oxazolinium ion intermediate with Asp142 treated as protonated, helping to stabilize the reaction species electrostatically,⁷ as proposed by Van Aalten et al.¹⁵ The second pathway (denoted as “path B”) is similar to path A and is consistent with the mechanism proposed for GH20 β -hexosaminidase,¹⁷ where an oxazolinium ion intermediate is formed in the reaction; however, in contrast to path A, Asp142 is treated as deprotonated and acts as a charged residue providing electrostatic stabilization of the oxazolinium intermediate. For the third pathway (denoted as “path C”), an alternative mechanism was proposed in which, Asp142, in conjunction with Glu144, acts as a proton-shuttle during hydrolysis, resulting in a mechanism which proceeds via an oxazoline intermediate similar to the one proposed to be formed in GH84 O-GlcNAcase¹⁶ and GH85 endohexosaminidases.¹² The free-energy profile for each path was calculated, and the results obtained are shown in Figure 3. Representative geometries of the QM region along the reaction pathway are also displayed. Geometric details of stationary structures, as

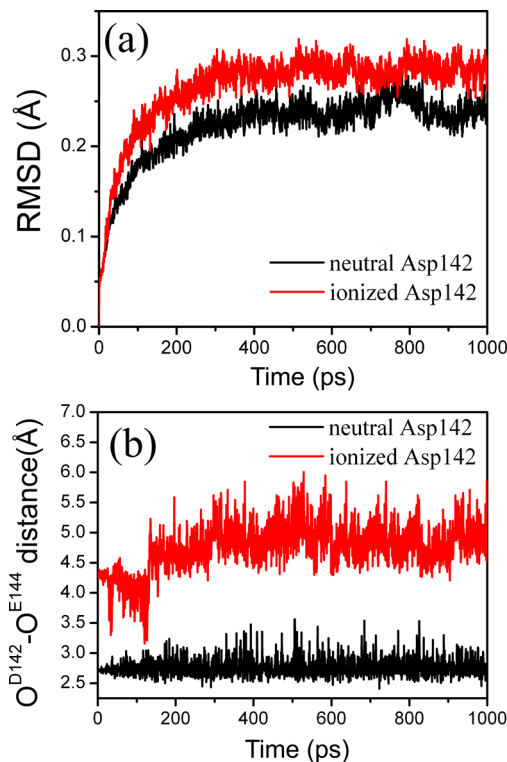


Figure 1. (a) RMSD of the protein heavy atoms and (b) Asp142 O δ 2 – Glu144 O ϵ 2 distance relative to the starting structure during 1 ns of QM/MM MD simulations of enzyme–substrate complex (ES) with neutral and ionized Asp142.

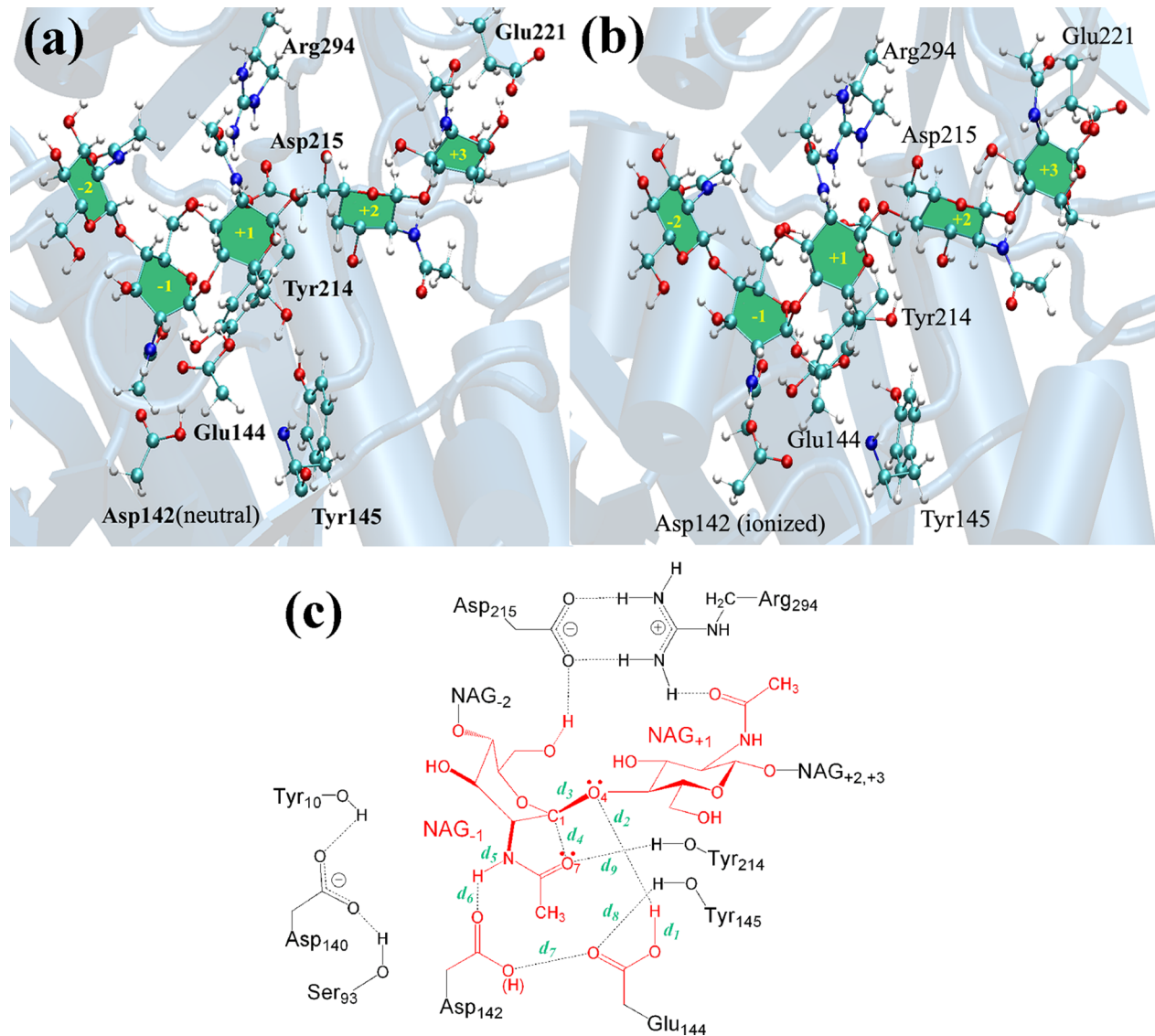


Figure 2. Snapshots of the equilibrated enzyme–substrate (ES) complex from QM/MM MD simulations containing (a) neutral and (b) ionized Asp142. (c) QM region for the glycosylation step (in red) and its structural parameters referred to in the text.

well as the conformations of the NAG moiety in subsite -1 along paths A–C, can be found in Table S2 and Figure S4 of the Supporting Information.

Mechanism via Oxazolinium-Ion Intermediate. Paths A and B both involve formation of an oxazolinium cation intermediate (in glycosylation) which then collapses upon hydrolysis (deglycosylation). In Figure 3 (panels a and b), it can be seen that the ES structures from paths A and B have similar geometries, with both displaying a twisted glycosidic bond linking the two glucosyl moieties in the -1 and $+1$ subsites. It was observed that a H-bonding network consisting of Asp142 and Glu144 helps to position the substrate in a reactive orientation within the active site. Additionally, a H-bond formed between Tyr214 and the acetamido group of the subsite -1 NAG residue (d_9) was also found to contribute to the distortion of this acetamido group. This distortion facilitates a reduction in the distance between the two atoms involved in the intramolecular nucleophilic attack ($d_4 = 2.83 \pm 0.06$ and 2.91 ± 0.05 Å for paths A and B, respectively) and thus helps to promote the first step of the reaction.

As shown in Figure 3a, three H-bonds are conserved throughout pathway A: Asp142 forms hydrogen bonds with the carboxylate group of Glu144 (d_7) and with the H–N bond of the acetamido group within the subsite -1 NAG (d_6) and Glu144 acts as a proton donor, forming a hydrogen bond to the scissile glycosidic linkage (d_2), with this later H-bond found to be formed at a shorter distance in path A (1.77 ± 0.09 Å) compared to the same H-bond observed in path B (1.85 ± 0.12 Å). The increased length of this H-bond, as observed in path B, coincided with the loss of the H-bond interaction between Glu144 and Asp142 (see Figure 3b). It therefore follows that the Asp142–Glu144 interaction must be present to enable the Glu144 to interact strongly with the substrate (supporting our previous conclusions made when investigating the D142N system).⁷ Additionally, these findings support our previous observations from adiabatic mapping that the presence of these H-bonds and their ability to stabilize the oxazolinium cation species electrostatically contribute to a lower reaction barrier.⁷

In the glycosylation step, two chemical processes were involved in the cleavage of the glycosidic bond. The formation of EI was found to be concerted but asynchronous in both

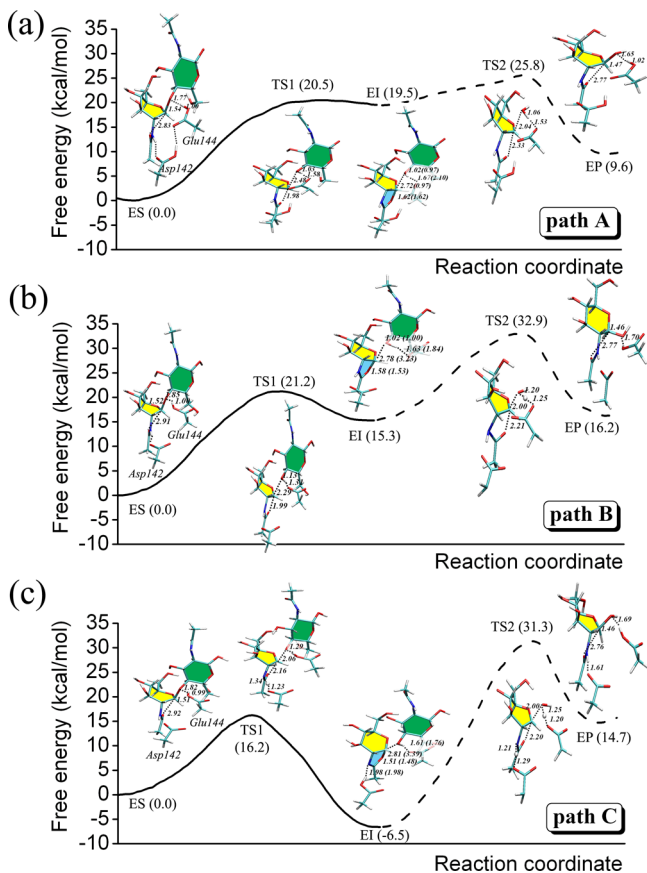


Figure 3. Free-energy profile for paths A–C calculated with QM/MM umbrella sampling MD. Representative geometries of the QM region at the stationary points (ES, TS1, EI, TS2, and EP) along the profile are displayed with important structural parameters labeled in units of Å. The unbroken line represents glycosylation, and the dashed line represents deglycosylation.

paths A and B. Starting from ES, Glu144 completely donates its proton to the glycosidic oxygen (d_2 ; 1.03 ± 0.03 Å for path A and 1.13 ± 0.03 Å for path B), while at the same time, the scissile glycosidic bond is cleaved to form TS1 (d_3 ; 2.48 ± 0.06 Å for path A and 2.29 ± 0.05 Å for path B). After this concerted step, it was observed that the covalent bond in TS1 between the N-acetyl nucleophile and the anomeric carbon is too large to be considered fully formed (d_4 ; 1.98 ± 0.06 Å for path A and 1.99 ± 0.05 Å for path B). Therefore, in an asynchronous process, intramolecular nucleophilic attack takes place, resulting in a narrowing of the N-acetyl oxygen and the anomeric carbon distance and the formation of the fused bicyclic ring found in the oxazolinium cation intermediate (EI). On the basis of the calculated geometries, the results indicate the reaction for paths A and B proceed first, with the transfer of the Glu144 proton onto the glycosidic oxygen before the oxazolinium intermediate is fully formed. Then, in a distinct step, nucleophilic addition of the N-acetyl oxygen at the anomeric center takes place, completing the formation of the intramolecular carbon–oxygen bond (d_4) and forming EI.

During the deglycosylation, the reverse process takes place. Nucleophilic attack of a water molecule at the anomeric center results in the collapse of the intermediate and the subsequent formation of the reaction product (EP). In TS2, the catalytic water was found to be positioned close to the anomeric carbon [d_3 ; 3.03 ± 0.07 Å (EI) → 2.04 ± 0.05 Å (TS2) for path A and

3.23 ± 0.06 Å (EI) → 2.00 ± 0.05 Å (TS2) for path B], while the fused oxazoline ring is spontaneously broken [d_4 ; 1.62 ± 0.07 Å (EI) → 2.33 ± 0.05 Å (TS2) for path A and 1.53 ± 0.04 Å (EI) → 2.21 ± 0.04 Å (TS2) for path B]. No proton abstraction was found at this stage in path A, as indicated by a distance of 1.53 ± 0.09 Å (d_1) between the water hydrogen and the Glu144 carboxylate oxygen, which is too large to be consistent with the formation of a bond. In contrast, path B indicates that proton abstraction between these two atoms had already taken place, with distances of 1.20 ± 0.01 Å and 1.25 ± 0.04 Å observed between the hydroxide water (OH^-) and its corresponding proton (d_2) and the same proton with the Glu144 carboxylate oxygen (d_1). These distances are representative of the formation of two transient bonds, indicating the transfer of a proton from the catalytic water onto the Glu144 residue. After TS2, in both paths A and B, the hydrogen abstraction was fully completed, resulting in the formation of the EP. The results of the calculation suggest that in path A the breakdown of the glycosidic linkage takes place prior to the proton abstraction of the water by Glu144, while these two steps are observed to be concerted in path B.

The calculated free-energy barriers for glycosylation and deglycosylation are 20.5 and 6.3 kcal/mol, respectively, for path A (Figure 3a) and 21.2 and 17.6 kcal/mol for path B (Figure 3b). For path A, an overall free-energy barrier of 25.8 kcal/mol was found, compared to a barrier of 32.9 kcal/mol determined for path B. These results therefore indicate that path A has a lower overall free-energy barrier to reaction. In the calculated free-energy profiles for both paths, deglycosylation was observed to be the rate-determining step in the reaction. The reactive conformation of the substrate was found to contain a glycosyl moiety at subsite –1, which was distorted away from its lowest-energy chair conformation. The conformation itinerary adopted by the NAG moiety at the subsite –1 of both pathways (Figure S4 of the Supporting Information) followed a boat (${}^1\text{B}_2$) → half-chair [${}^4\text{H}_5$ ‡] → chair (${}^4\text{C}_1$) pattern for glycosylation. However, for deglycosylation the conformational changes of the moiety in the –1 subsite for path A, chair (${}^4\text{C}_1$) → half-chair [${}^4\text{H}_5$ ‡] → boat (${}^1\text{B}_2$), was different from path B, chair (${}^4\text{C}_1$) → boat [${}^{2,5}\text{B}$]‡ → chair (${}^2\text{C}_5$), despite both pathways following a similar reaction mechanism.

The calculated energies and observed conformational itineraries for the reaction profiles showed that the major difference between paths A and B (and therefore the impact of a protonated Asp142 compared to a deprotonated Asp142) was in the deglycosylation step of the reaction. The smaller overall free-energy barrier calculated for the reaction proceeding via path A could be attributed to the reaction taking place through a lower-energy transition state (TS2) compared to the one observed in path B. This energy difference is likely due to the stronger H-bond network formed by residues Asp142, Glu144, the catalytic water, and the H–N bond of the acetamido group (d_1 , d_6 , d_7 ; Figure 2c) with these interactions providing more stabilization of the half-chair glycosyl moiety in TS2 of path A than the boat conformation formed in path B. These geometric observations are supported by the stabilization calculations performed on the system (Figure S5 of the Supporting Information) that show that the enzyme provides ~5 kcal/mol of stabilization of the reaction in enzyme in path A compared to minimal stabilization observed in path B.

In contrast, in the glycosylation step of the reaction, path B, despite representing a less energetically favored overall pathway and greater barrier to glycosylation, indicated that the

unprotonated Asp142 stabilized the oxazolinium ion species (EI) more effectively than the protonated Asp142 in path A (presumably because of the ion–ion interaction between the negative charge of the ionized Asp142 and the developing positive charge of the oxazolinium intermediate). Consequently, a shorter d_6 distance at the EI (EI1/EI2) was observed for path B (1.41–1.58 Å, Table S2 of the Supporting Information) compared to path A (1.60–1.77 Å, Table S2 of the Supporting Information). These findings therefore provide some evidence to explain why the analogous residue to Asp142 in similar GHs (GH20) is believed to be deprotonated in the active enzyme.^{17,22}

Mechanism via Oxazoline Intermediate. In contrast to paths A and B, path C consists of a mechanism that proceeds via an oxazoline intermediate with both Asp142 and Glu144 acting as the catalytic acid/base residues. The calculated energies and geometries for path C are shown in Figure 3c. The starting geometries of the substrate and active site residues in path C are almost identical to that observed in path B, as would be expected due to both systems containing Asp142 in the same protonation state. During the glycosylation, cleavage of the glycosidic bond was found to occur concomitantly with the proton abstraction by Asp142 (which acts as a general base) from the H–N bond of the acetamido group at the NAG subsite –1. This event is likely to be assisted by the H-bond polarization at the glycosidic bond by Glu144. Additionally, it was observed in TS1 that two transient bonds ($d_5 = 1.34 \pm 0.01$ and $d_6 = 1.23 \pm 0.04$ Å) between the acetamido group and the Asp142 carboxylate oxygen, and a further two transient bonds ($d_3 = 2.06 \pm 0.04$ and $d_4 = 2.16 \pm 0.04$ Å) between three atoms of the glycosidic oxygen, anomeric carbon, and carbonyl oxygen were formed, indicating that the Glu144 proton had not transferred fully onto the oxygen in the scissile glycosidic bond. After TS1, the Glu144 proton is fully transferred onto the cleaved glycosidic oxygen and the acetamido proton is bonded to the Asp142 carboxylate oxygen, leading to the formation of the oxazoline intermediate. In deglycosylation, the aglycon leaving group is removed and the nucleophilic attack of the oxazoline intermediate was performed. In this final step of the reaction, proton abstraction from a water molecule by Glu144 occurs concomitant with the proton transfer from Asp142 to the acetamido group, indicated by d_1 , d_2 , d_5 , d_6 distances in the range of 1.20–1.29 Å observed in TS2 (see Figure 3c). On completion of the deglycosylation step, EP is obtained, consisting of a substrate which has retained the original stereochemistry of its anomeric carbon with respect to the reactant, as observed for paths A and B.

The calculated free-energy barriers for glycosylation and deglycosylation are 16.2 and 37.8 kcal/mol, respectively. Deglycosylation, as observed in paths A and B, was found to be the rate-determining step in the free-energy profile calculated for path C. The conformation of the ring in the –1 subsite in path C was found to adopt boat ($^{1,4}B$) → half-chair [4H_5] \ddagger → chair (3C_2) for the glycosylation, and chair (3C_2) → boat [$B_{2,5}$] \ddagger → boat ($B_{2,5}$) for the deglycosylation.

Why is Path A Energetically Favored? Comparison of SCC-DFTB and B3LYP Results. From our calculations, path A has the lowest free-energy barrier (25.8 kcal/mol) of the three pathways modeled, with paths B and C calculated to have overall barriers of 32.9 and 31.3 kcal/mol, respectively. The barriers for each step of the reaction (glycosylation and deglycosylation) differ significantly among the three pathways with deglycosylation found to have the most variation in barrier

height; it is also predicted to be the likely rate-determining step of the reaction. The barrier to glycosylation was lowest in path C (16.2 kcal/mol) followed by paths A (20.5 kcal/mol) and B (21.2 kcal/mol). In contrast, the barrier to deglycosylation (calculated as the difference in energy between TS2 and EI2) was lowest in path A (6.3 kcal/mol) followed by paths B (17.6 kcal/mol) and C (37.8 kcal/mol). Path A therefore represents the most energetically favorable pathway for the ChiB-catalyzed reaction, with a free-energy barrier of 25.8 kcal/mol. This is significantly higher than the experimentally derived barrier of 16.1 kcal/mol ($k_{cat} = 28 \text{ s}^{-1}$); this is probably due to limitations of the SCC-DFTB QM method used in the calculations.⁴⁸

Small model, single-point (SP) calculations utilizing a higher level of theory (B3LYP) were used to estimate the relative accuracy of the energies calculated with the SCC-DFTB method. In order to perform this comparison, representative geometries of the QM region of the stationary points found along the SCC-DFTB/MM free-energy paths A to C were extracted. SP calculations were then performed on each of these structures with SCC-DFTB and B3LYP to compare the relative energies of the structures calculated with the different methods. Additionally, the basis set dependence of the B3LYP-calculated energies was assessed by performing SP B3LYP calculations with a variety of different-sized basis sets: 6-31G(d), 6-31G(d,p), and 6-311+G(d,p) (Table 1).

The SP corrections performed on path A show that the relative energies of the stationary points representing TS1 and TS2 obtained with SCC-DFTB are in good agreement with

Table 1. Comparison of Relative Potential Energies (in kcal/mol) of the QM Region at the Six Stationary Points (ES, TS1, EI1, EI2, TS2, and EP) for Both Glycosylation and Deglycosylation Among Three Reaction Pathways (A, B, and C)^a

path:methods	glycosylation			deglycosylation		
	ES	TS1	EI1	EI2	TS2	EP
path A: US(SCC-DFTB/CHARMM)	0.0	20.5	19.5	0.0	6.3	-9.9
SP(SCC-DFTB)	0.0	19.7	13.9	0.0	11.6	-11.8
SP[B3LYP/6-31G(d)]	0.0	19.2	7.9	0.0	9.5	-15.6
SP[B3LYP/6-31G(d,p)]	0.0	17.7	5.9	0.0	10.3	-14.1
SP[B3LYP/6-311+G(d,p)]	0.0	17.1	4.7	0.0	11.4	-11.2
path B: US(SCC-DFTB/CHARMM)	0.0	21.2	15.3	0.0	17.6	0.9
SP(SCC-DFTB)	0.0	32.8	28.7	0.0	21.2	-5.2
SP[B3LYP/6-31G(d)]	0.0	29.3	22.8	0.0	21.0	-9.5
SP[B3LYP/6-31G(d,p)]	0.0	28.0	22.3	0.0	21.0	-8.1
SP[B3LYP/6-311+G(d,p)]	0.0	27.3	20.2	0.0	20.7	-6.6
path C: US(SCC-DFTB/CHARMM)	0.0	16.2	-6.5	0.0	37.8	21.2
SP(SCC-DFTB)	0.0	21.9	5.4	0.0	27.2	-3.2
SP[B3LYP/6-31G(d)]	0.0	30.0	9.5	0.0	25.0	-5.5
SP[B3LYP/6-31G(d,p)]	0.0	28.4	8.8	0.0	23.3	-5.6
SP[B3LYP/6-311+G(d,p)]	0.0	28.7	7.4	0.0	26.5	-2.1
exptl ^a				16.1		

^aActivation energy as estimated from the experimental rate of reaction⁴⁸ by using transition state theory. ^bValues are single-point (SP) energies calculated at SCC-DFTB and B3LYP with a different basis set. Umbrella sampling (US) QM/MM free energies are also included for comparison.

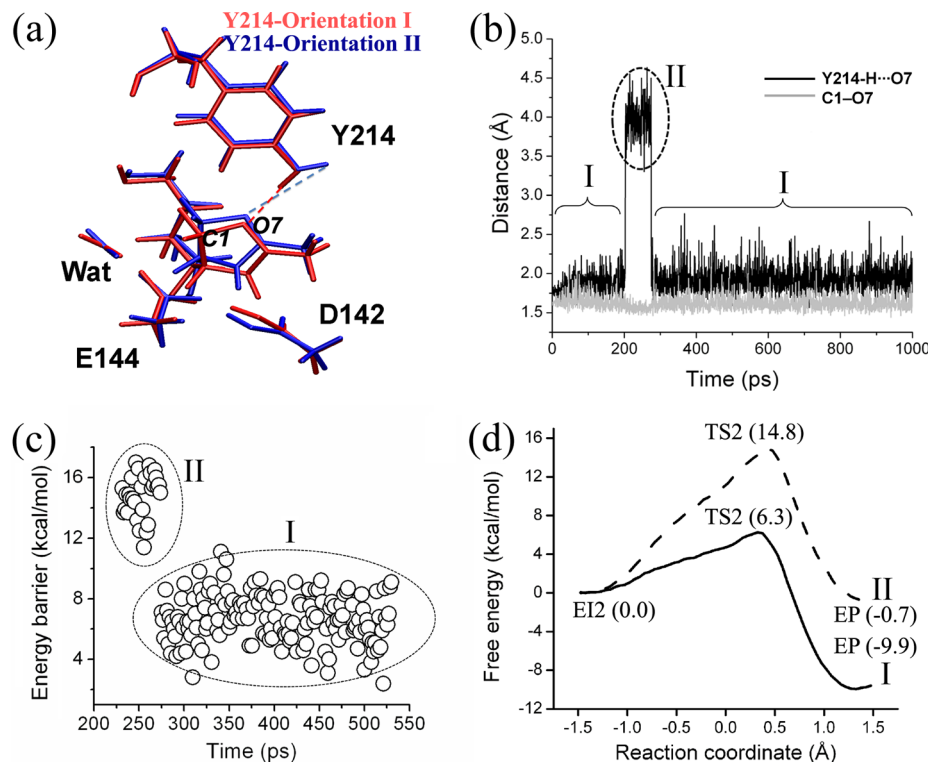


Figure 4. Analysis of Tyr214 in the deglycosylation step of ChiB catalysis. (a) Schematic representation of orientations adopted by Tyr214 with (I) and without (II) the hydrogen bond to the oxygen in the oxazolinium ring. (b) Relevant distances ($\text{Y214}-\text{H}\cdots\text{O}7$ and $\text{C1}-\text{O}7$) related to the two orientations adopted by Tyr214 during 1 ns QM/MM MD simulation. (c) Clusters of calculated potential-energy barriers to deglycosylation (SCC-DFTB/CHARMM22) for selected snapshots extracted between 200 and 500 ps during QM/MM MD simulations. (d) Calculated free-energy profile (for deglycosylation) with Tyr214 in orientations I and II.

B3LYP/6-31G(d). SCC-DFTB was found to only slightly overestimate the energy of these two points by 0.5 and 2.1 kcal/mol for TS1 and TS2, respectively, indicating it is a reasonably accurate method for estimating the relative barriers for the glycosylation and deglycosylation steps.

For paths B and C, the B3LYP/6-31G(d) relative energies calculated for TS2 are also found to be in good agreement with SCC-DFTB (with a difference of 0.2 and 2.2 kcal/mol between the methods for paths B and C, respectively), while a larger correction was observed when comparing the energies obtained for TS1. These corrections show, first, that the SCC-DFTB calculated barriers to glycosylation for these paths are not consistent with the higher level of theory and, second, despite the difference in the relative energies of TS2 calculated by the two methods, the correction to the TS2 energy has no significant influence on the overall barrier to reaction. This is because, despite accounting for the large correction to the TS2 energy, deglycosylation is still found to be the rate-limiting step for both paths. Consequently, the overall conclusions drawn from analyzing the SCC-DFTB/MM calculated free-energy profiles are still valid.

In contrast, the SP calculations performed to correct the relative energy of EI1, formed after the glycosylation step, has significant implications in the analysis of the free-energy profile obtained for path A. The SP B3LYP energy for EI1 shows that SCC-DFTB overestimates the relative energy of the intermediate by 6.0 kcal/mol. Therefore, accounting for the fact the EI1 is calculated to be more stable with the higher level of theory but recognizing SCC-DFTB accurately calculates the relative barrier to deglycosylation, the correction shows that glycosylation, and not deglycosylation, is in fact the rate-

determining step of reaction in path A. This is because correcting the SCC-DFTB energy of EI1 now lowers the energy of TS2 relative to ES, resulting in TS1 now representing a structure with the highest relative energy on the reaction pathway.

For paths B and C, despite SP calculations showing similar discrepancies for the calculated relative energies of EI1 between two methods, the paths exhibit either a significantly higher barrier for deglycosylation [path C, TS2:25.0 kcal/mol B3LYP/6-31G(d)] or a higher-energy intermediate (path B, EI1:22.8 kcal/mol). As a result, although SCC-DFTB overestimates the energy of EI1 compared with B3LYP, the correction to the SCC-DFTB energy would not be enough to stabilize TS2 such that it is lower in energy than TS1 in paths B and C. Consequently, deglycosylation remains as the rate-determining step for both of these paths with a slight increase in the height of the overall barrier to reaction for path C (by 2.1 kcal/mol).

In summary, the corrections indicate path A is still the most energetically favorable pathway but importantly indicate that glycosylation, and not deglycosylation, is in fact the rate-limiting step of the reaction due to SCC-DFTB overestimating the energy of EI1 in the free-energy profiles obtained previously. Further support for this conclusion is provided by a comparison of the free-energy profiles for the wild-type and mutant (D142N) reactions. The results (Figure S6 of the Supporting Information) from these calculations indicate that mutation affects the glycosylation step most significantly, with a relatively high free-energy barrier calculated for the glycosylation step in the mutant compared with the barrier in the wild-type. This finding is in line with experimental studies that

have shown the D142N mutant catalyzes the reaction less efficiently than the wild-type.²¹

SP calculations with different basis sets indicate that there is a small dependence of the calculated energy with respect to the size of the basis set used for the B3LYP calculation. Calculating the standard deviation of the B3LYP energies of each of the stationary points for the three paths indicates that the largest basis set dependence was observed for the energy of EI1 in path A ($\sigma = 1.6$ kcal/mol) and the lowest for energy of TS2 in path B ($\sigma = 0.2$ kcal/mol). It was also found that increasing the size of basis set used in the calculation resulted in a lowering of the overall barrier to reaction, with a decrease of 2.1, 2.9, and 0.6 kcal/mol for paths A, B, and C, respectively, when increasing the basis used for the calculation from 6-31G(d) to 6-311+ +G(d,p). This shows that an increase in the size of the basis set used, as well as employing a higher level theory to calculate the energy of the QM region, would likely result in a lower free-energy barrier to be calculated for the reaction, thus improving the agreement with the experimental calculated barrier of 16.1 kcal/mol.

Catalytic Importance of Tyr214. To better understand the role of Tyr214 in the reaction, further analysis was performed on the EI2 complex (with neutral Asp142) by running a 1 ns QM/MM MD simulation in order to assess its stability and examine the influence of the H-bond formed by Tyr214. The RMSD plot from the simulation, shown in Figure S7 of the Supporting Information, indicates a stable MD trajectory was obtained after 200 ps. Interestingly, during the 1 ns simulation, two different orientations (I and II) of Tyr214 were unexpectedly observed (Figure 4, panels a and b): one conformation (I) in which the residue could form a hydrogen bond with the oxazolinium oxygen (observed between 0–200 ps and 300–1000 ps) and the other (II), where its side-chain pointed away from the substrate (observed between 200–300 ps). To analyze the impact of the reorientation of the Tyr214 on the reaction energetics, several snapshots representing one of the two observed orientations, I and II, were chosen from the QM/MM MD and used as a starting structure for reaction modeling. In a similar manner as performed previously, umbrella sampling MD based on adiabatic mapping was then performed on the extracted snapshots in order to simulate reaction pathway A. II was not observed in any previous MD simulations on the ES complex (Figure 5a), and therefore, a restraint was imposed on the system to ensure a H-bond distance between the acetamido O7 oxygen of subsite -1 NAG and the hydroxyl group of Tyr214 could not be formed. This allowed II to be formed in ES and ensured that this orientation was maintained during the simulation of the glycosylation step of the reaction.

The calculations showed that different orientations of the Tyr214 resulted in significantly different reaction barriers for the reaction (Figures 4c and 5b). The deglycosylation step of the reaction was found to be most affected by this change in orientation, with a calculated free-energy barrier relative to the intermediate (EI1) of 6.3 and 14.8 kcal/mol, for I and II, respectively (Figure 4d). In contrast, the glycosylation step was affected less by the reorientation, with a calculated barrier to glycosylation of 20.5 kcal/mol compared to 16.7 kcal/mol for I and II, respectively. These calculations reveal new insight to the importance of the Tyr214 residue and specifically the influence of this H-bond with the substrate on each individual step of the enzyme-catalyzed reaction.

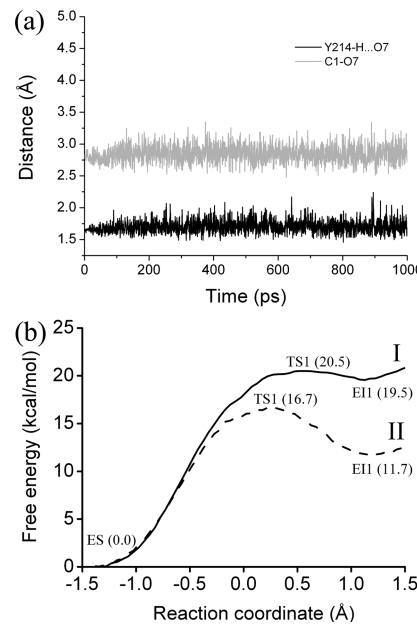


Figure 5. Analysis of Tyr214 in the glycosylation step of ChiB catalysis. (a) Relevant distances (Y214-H...O7 and C1-O7) related to the two orientations adopted by Tyr214 during 1 ns QM/MM MD simulation. (b) Calculated free-energy profile (for glycosylation) with Tyr214 in orientations I and II.

In glycosylation, the presence of the Tyr214 H-bond (I) results in a higher barrier for the formation of the oxazolinium ion. This is probably due to the H-bond interacting with and reducing the nucleophilicity of the O7 oxygen, as well as hindering the movement of nucleophilic oxygen as the C1-O7 NAG distance is reduced during intramolecular nucleophilic attack. Conversely, in deglycosylation, the H-bond is shown to have an opposite and greater effect on the barrier to reaction (Figure 5). In I, the relative energy of EI1 indicates that the Tyr214 H-bond acts to destabilize the oxazolinium ion intermediate and, as a result, this lowers the barrier to deglycosylation (by 8.5 kcal/mol). In II, in the absence of the Tyr214 H-bond, the destabilizing effect on EI1 is not observed and the barrier of the deglycosylation step is raised and results in deglycosylation now becoming the rate-limiting step of the reaction. These free-energy calculations performed with I and II show that, although the Tyr214 influences the efficiency of the glycosylation step, it plays a more vital role in the deglycosylation step of the reaction, reducing the barrier of this step such that it is no longer rate-determining. This subtle observation provides new evidence to explain the origin of the reduced rate observed in the Y214F mutant observed in the experiment, as well as its analogous residue in other GH enzymes, and confirms previous stabilization calculations performed on the system that showed that the Tyr214 H-bond destabilizes the transition state and enzyme intermediate in the glycosylation step of the reaction.⁷

QM/MM MD Simulations of Enzyme–Product Complex. To gain further insight into the dynamics and stability of the enzyme–product complex after the catalytic reaction, two additional QM/MM MD simulations with different semi-empirical treatments of the QM region (i.e., SCC-DFTB/CHARMM22 and AM1/CHARMM22) were performed. The RMSD plots for the heavy atoms in the enzyme–product complex indicate that both simulations are reasonably stable

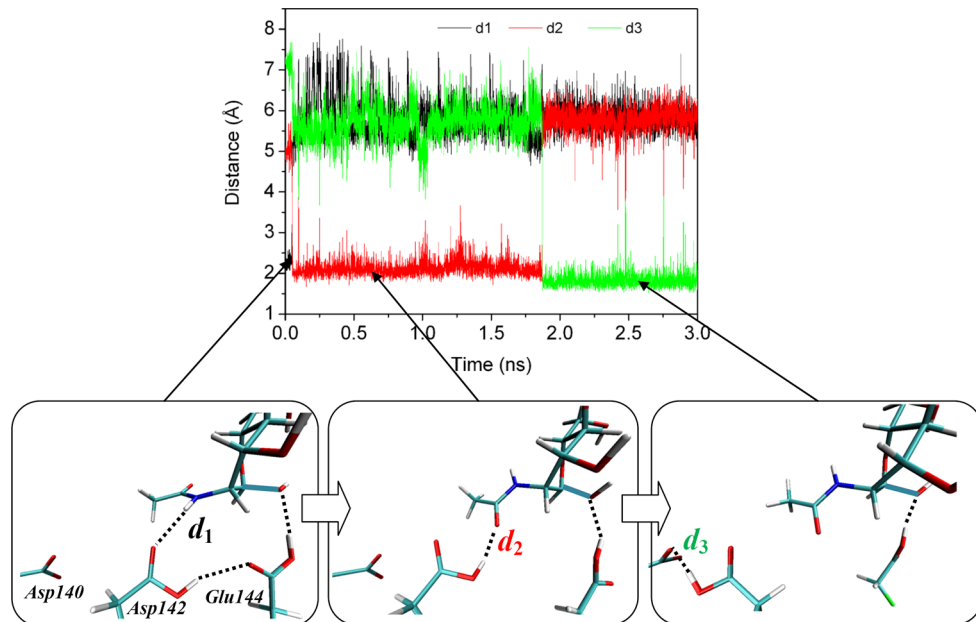


Figure 6. Snapshots showing the important conformational changes associated with the product unbinding event observed in the AM1/CHARMM22 MD simulation on the enzyme–product complex. $d_1 = \text{HN}2-\text{Oe}2(\text{Asp}142)$, $d_2 = \text{O}7-\text{He}2(\text{Asp}142)$, and $d_3 = \text{Oe}2(\text{Asp}140)-\text{He}2(\text{Asp}142)$.

(Figure S8 of the Supporting Information). The simulation performed with SCC-DFTB/CHARMM22 reached an equilibrated structure faster than in the AM1/CHARMM22 MD (indicated by low RMSD, Figure S8 of the Supporting Information). A difference in the binding stability of the products was also observed. In the SCC-DFTB/CHARMM22 simulation, Asp142, Glu144, and Tyr214 were found to bind the reaction product more tightly at the -2 and -1 binding subsites of the enzyme ($d_2 = 1.64 \pm 0.01 \text{ \AA}$, $d_6 = 1.98 \pm 0.16 \text{ \AA}$, and $d_9 = 1.73 \pm 0.11 \text{ \AA}$) compared to the binding observed in the AM1/CHARMM22 simulation ($d_2 = 2.09 \pm 0.01 \text{ \AA}$, $d_6 = 5.75 \pm 0.61 \text{ \AA}$, and $d_9 = 4.64 \pm 0.75 \text{ \AA}$). Furthermore, the AM1/CHARMM22 simulation contained an interesting unbinding event, where the Asp142 side chain rotated in, allowing the N -acetyl group of subsite -1 NAG to flip its orientation, thus facilitating the release of the product (Figure 6). The boat conformation was observed at subsite -1 during the simulation. This observation provides further evidence to support the role of the $-OH$ group on Tyr214 and Asp142 in contributing to the distortion of the N -acetyl group of the -1 subsite NAG and underlines the importance of their interactions in contributing to the binding of the substrate.

CONCLUSIONS

In this study, the QM/MM umbrella sampling MD free-energy simulations have been performed on the unusual substrate-assisted mechanism of *S. marcescens* ChiB. The contribution of two conserved amino acid residues, Asp142 and Tyr214, to enzyme catalysis was investigated. In particular, the role of Asp142, and the influence of its protonation state on the reaction mechanism⁷ were examined through the three different reaction pathways modeled (paths A–C), treating the residue as either ionized or neutral. Our simulations show that the system containing a neutral Asp142 residue stabilizes the transition state of the deglycosylation step more effectively than in the other paths (outweighing the observed destabilization of the transition state in the glycosylation step). This resulted in

the lowest overall free-energy barrier among the three pathways to be calculated for path A, supporting our previous theoretical study and in agreement with experimental findings^{7,15} and underlining the important contribution of the Asp142 in the second step of the reaction. Analysis of two different possible orientations of Tyr214 enabled the important role of the H-bond formed by the residue with the substrate to be investigated. Our results showed that the interaction was necessary to facilitate efficient deglycosylation and prevent it from being the rate-limiting step in the reaction.

Small model, single point B3LYP calculations with a variety of different-sized basis sets indicated that SCC-DFTB overestimates the destabilization of the intermediate formed in the enzyme-catalyzed reaction. This emphasized the importance of validating semiempirical methods with higher level methods and provided evidence to suggest that glycosylation and not deglycosylation was the rate-determining step of the reaction.

A complex conformational change of the chitose unit in the subsite -1 along the reaction pathway was found to take place adopting boat (${}^1\text{A}_1$) \rightarrow half-chair [${}^4\text{H}_5$] ‡ \rightarrow chair (${}^4\text{C}_1$) for the glycosylation step and the reverse conformations for deglycosylation: chair (${}^4\text{C}_1$) \rightarrow half-chair [${}^4\text{H}_5$] ‡ \rightarrow boat (${}^1\text{A}_1$). Further QM/MM MD simulations of the enzyme–product complex were also performed in which an unbinding event is suggested to have been captured, affording new mechanistic insight into the release of the product of ChiB.

ASSOCIATED CONTENT

S Supporting Information

Position of the nucleophilic water for the deglycosylation from QM/MM MD (Figure S1); definition of the reaction coordinate used in this work (Figure S2); snapshot of the ES complex when Asp142 is ionized (Figure S3); distorted conformations of NAG subsite -1 along the reaction coordinate of paths A–C (Figure S4); calculated stabilization energy profiles for paths A–C along the reaction coordinate of glycosylation and deglycosylation steps (Figure S5); free-energy

profiles for the D142N mutant (Figure S6); RMSD curves from the QM/MM simulations of the EI2 and EP complex of path A (Figures S7 and S8); geometric parameters for ES snapshots of both neutral and ionized Asp142 models (Table S1) and for stationary points along the reaction coordinates of paths A–C (Table S2). This material is available free of charge via the Internet at <http://pubs.acs.org>.

AUTHOR INFORMATION

Corresponding Author

*E-mail: jitrayut.018@gmail.com. Tel: +66 (0) 5446 6666, ext. 1834. Fax: +66 (0) 5446 6664.

Notes

The authors declare no competing financial interest.

ACKNOWLEDGMENTS

This work was carried out within the Research Grant for New Scholar (Grant MRG5680143) that is cofunded by the Thailand Research Fund, the Office of the Higher Education Commission, and the University of Phayao, Thailand. J.J. thanks Prof. Supa Hannongbua for her kind support and guidance of this research project. We thank Dr. Joni Mujika, Dr. Julianna Oláh, and Dr. Christoph Sontag for their critical reading of the manuscript. A.J.M. is an EPSRC Leadership Fellow and thanks EPSRC for support (Grant EP/G007705/1). A.J.M. and M.A.L. thank EPSRC and BBSRC for support. This research was also funded by the University of Phayao (Grant R020056216016).

REFERENCES

- (1) Carbohydrates and Glycobiology. *Science* **2001**, *291*, 2263–2502.
- (2) Wolfenden, R.; Lu, X. D.; Young, G. Spontaneous Hydrolysis of Glycosides. *J. Am. Chem. Soc.* **1998**, *120*, 6814–6815.
- (3) Cantarel, B. L.; Coutinho, P. M.; Rancurel, C.; Bernard, T.; Lombard, V.; Henrissat, B. The Carbohydrate-Active Enzymes Database (CAZy): An Expert Resource for Glycogenomics. *Nucleic Acids Res.* **2009**, *37*, D233–D238.
- (4) Koshland, D. E. Stereochemistry and the Mechanism of Enzymatic Reactions. *Biol. Rev.* **1953**, *28*, 416–436.
- (5) Vocadlo, D. J.; Davies, G. J. Mechanistic Insights into Glycosidase Chemistry. *Curr. Opin. Chem. Biol.* **2008**, *12*, 539–555.
- (6) Vuong, T. V.; Wilson, D. B. Glycoside Hydrolases: Catalytic Base/Nucleophile Diversity. *Biotechnol. Bioeng.* **2010**, *107*, 195–205.
- (7) Jittonnom, J.; Lee, V. S.; Nimmanipug, P.; Rowlands, H. A.; Mulholland, A. J. Quantum Mechanics/Molecular Mechanics Modeling of Substrate-Assisted Catalysis in Family 18 Chitinases: Conformational Changes and the Role of Asp142 in Catalysis in ChiB. *Biochemistry* **2011**, *50*, 4697–4711.
- (8) Vocadlo, D. J.; Davies, G. J.; Laine, R.; Withers, S. G. Catalysis by Hen Egg-White Lysozyme Proceeds Via a Covalent Intermediate. *Nature* **2001**, *412*, 835–839.
- (9) Vocadlo, D. J.; Mayer, C.; He, S.; Withers, S. G. Mechanism of Action and Identification of Asp242 as the Catalytic Nucleophile of *Vibrio furnisii* N-Acetyl- β -D-Glucosaminidase Using 2-Acetamido-2-Deoxy-5-Fluoro- α -L-Idopyranosyl Fluoride. *Biochemistry* **2000**, *39*, 117–126.
- (10) Huet, J.; Rucktooa, P.; Clantin, B.; Azarkan, M.; Looze, Y.; Villeret, V.; Wintjens, R. X-ray Structure of Papaya Chitinase Reveals the Substrate Binding Mode of Glycosyl Hydrolase Family 19 Chitinases. *Biochemistry* **2008**, *47*, 8283–8291.
- (11) Tvaroska, I.; Kozmon, S.; Wimmerova, M.; Koca, J. Substrate-Assisted Catalytic Mechanism of O-GlcNAc Transferase Discovered by Quantum Mechanics/Molecular Mechanics Investigation. *J. Am. Chem. Soc.* **2012**, *134*, 15563–15571.
- (12) Abbott, D. W.; Macauley, M. S.; Vocadlo, D. J.; Boraston, A. B. Streptococcus pneumoniae Endohexosaminidase D, Structural and Mechanistic Insight into Substrate-Assisted Catalysis in Family 85 Glycoside Hydrolases. *J. Biol. Chem.* **2009**, *284*, 11676–11689.
- (13) Macauley, M. S.; Whitworth, G. E.; Debowski, A. W.; Chin, D.; Vocadlo, D. J. O-GlcNAcase Uses Substrate-Assisted Catalysis: Kinetic Analysis and Development of Highly Selective Mechanism-Inspired Inhibitors. *J. Biol. Chem.* **2005**, *280*, 25313–25322.
- (14) Mark, B. L.; Vocadlo, D. J.; Knapp, S.; Triggs-Raine, B. L.; Withers, S. G.; James, M. N. Crystallographic Evidence for Substrate-Assisted Catalysis in a Bacterial β -Hexosaminidase. *J. Biol. Chem.* **2001**, *276*, 10330–10337.
- (15) Van Aalten, D. M. F.; Komander, D.; Synstad, B.; Gaseidnes, S.; Peter, M. G.; Eijsink, V. G. H. Structural Insights into the Catalytic Mechanism of a Family 18 Exo-Chitinase. *Proc. Natl. Acad. Sci. U.S.A.* **2001**, *98*, 8979–8984.
- (16) Bottoni, A.; Pietro Mischione, G.; Calvaresi, M. Computational Evidence for the Substrate-Assisted Catalytic Mechanism of O-GlcNAcase. A DFT Investigation. *Phys. Chem. Chem. Phys.* **2011**, *13*, 9568–9577.
- (17) Passos, Ó.; Fernandes, P.; Ramos, M. Theoretical Insights into the Catalytic Mechanism of β -Hexosaminidase. *Theor. Chem. Acc.* **2011**, *129*, 119–129.
- (18) Andersen, O. A.; Dixon, M. J.; Eggleston, I. M.; van Aalten, D. M. Natural Product Family 18 Chitinase Inhibitors. *Nat. Prod. Rep.* **2005**, *22*, 563–579.
- (19) Houston, D. R.; Synstad, B.; Eijsink, V. G.; Stark, M. J.; Eggleston, I. M.; van Aalten, D. M. Structure-Based Exploration of Cyclic Dipeptide Chitinase Inhibitors. *J. Med. Chem.* **2004**, *47*, 5713–5720.
- (20) Horn, S. J.; Sikorski, P.; Cedervist, J. B.; Vaaje-Kolstad, G.; Soerlie, M.; Synstad, B.; Vriend, G.; Vaerum, K. M.; Eijsink, V. G. H. Costs and Benefits of Processivity in Enzymatic Degradation of Recalcitrant Polysaccharides. *Proc. Natl. Acad. Sci. U.S.A.* **2006**, *103*, 18089–18094.
- (21) Synstad, B.; Gaseidnes, S.; van Aalten, D. M. F.; Vriend, G.; Nielsen, J. E.; Eijsink, V. G. H. Mutational and Computational Analysis of the Role of Conserved Residues in the Active Site of a Family 18 Chitinase. *Eur. J. Biochem.* **2004**, *271*, 253–262.
- (22) Williams, S. J.; Mark, B. L.; Vocadlo, D. J.; James, M. N. G.; Withers, S. G. Aspartate 313 in the Streptomyces plicatus Hexosaminidase Plays a Critical Role in Substrate-Assisted Catalysis by Orienting the 2-Acetamido Group and Stabilizing the Transition State. *J. Biol. Chem.* **2002**, *277*, 40055–40065.
- (23) Cetinbas, N.; Macauley, M. S.; Stubbs, K. A.; Drapala, R.; Vocadlo, D. J. Identification of Asp174 and Asp175 as the Key Catalytic Residues of Human O-GlcNAcase by Functional Analysis of Site-Directed Mutants. *Biochemistry* **2006**, *45*, 3835–3844.
- (24) Papanikolau, Y.; Prag, G.; Taylas, G.; Vorgias, C. E.; Oppenheim, A. B.; Petratos, K. High Resolution Structural Analyses of Mutant Chitinase a Complexes with Substrates Provide New Insight into the Mechanism of Catalysis. *Biochemistry* **2001**, *40*, 11338–11343.
- (25) Bokma, E.; Rozeboom, H. J.; Sibbald, M.; Dijkstra, B. W.; Beintema, J. J. Expression and Characterization of Active Site Mutants of Hevamine, a Chitinase from the Rubber Tree Hevea brasiliensis. *Eur. J. Biochem.* **2002**, *269*, 893–901.
- (26) Hsieh, Y. C.; Wu, Y. J.; Chiang, T. Y.; Kuo, C. Y.; Shrestha, K. L.; Chao, C. F.; Huang, Y. C.; Chuankhayan, P.; Wu, W. G.; Li, Y. K.; Chen, C. J. Crystal Structures of *Bacillus cereus* NCTU2 Chitinase Complexes with Chitoooligomers Reveal Novel Substrate Binding for Catalysis: A Chitinase without Chitin Binding and Insertion Domains. *J. Biol. Chem.* **2010**, *285*, 31603–31615.
- (27) Houston, D. R.; Shiomi, K.; Arai, N.; Omura, S.; Peter, M. G.; Turberg, A.; Synstad, B.; Eijsink, V. G.; van Aalten, D. M. High-Resolution Structures of a Chitinase Complexed with Natural Product Cyclopentapeptide Inhibitors: Mimicry of Carbohydrate Substrate. *Proc. Natl. Acad. Sci. U.S.A.* **2002**, *99*, 9127–9132.
- (28) Houston, D. R.; Eggleston, I.; Synstad, B.; Eijsink, V. G. H.; van Aalten, D. M. F. The Cyclic Dipeptide Cl-4 [Cyclo-(L-Arg-D-Pro)] Inhibits Family 18 Chitinases by Structural Mimicry of a Reaction Intermediate. *Biochem. J.* **2002**, *368*, 23–27.

- (29) Bas, D. C.; Rogers, D. M.; Jensen, J. H. Very Fast Prediction and Rationalization of pKa Values for Protein-Ligand Complexes. *Proteins: Struct., Funct., Bioinf.* **2008**, *73*, 765–783.
- (30) Vriend, G. WHAT IF: A Molecular Modeling and Drug Design Program. *J. Mol. Graphics* **1990**, *8*, 52–56.
- (31) Brooks, B. R.; Brucoleri, R. E.; Olafson, B. D.; States, D. J.; Swaminathan, S.; Karplus, M. CHARMM: A Program for Macromolecular Energy, Minimization, and Dynamics Calculations. *J. Comput. Chem.* **1983**, *4*, 187–217.
- (32) Elstner, M.; Porezag, D.; Jungnickel, G.; Elsner, J.; Haugk, M.; Frauenheim, T.; Suhai, S.; Seifert, G. Self-Consistent-Charge Density-Functional Tight-Binding Method for Simulations of Complex Materials Properties. *Phys. Rev. B* **1998**, *58*, 7260–7268.
- (33) Cui, Q.; Elstner, M.; Kaxiras, E.; Frauenheim, T.; M, K. A QM/MM Implementation of the Self-Consistent Charge Density Functional Tight Binding (SCC-DFTB) Method. *J. Phys. Chem. B* **2001**, *105*, 569–585.
- (34) Liu, J.; Wang, X.; Xu, D. QM/MM Study on the Catalytic Mechanism of Cellulose Hydrolysis Catalyzed by Cellulase Cel5A from Acidothermus cellulolyticus. *J. Phys. Chem. B* **2010**, *114*, 1462–1470.
- (35) Xu, D.; Guo, H. Quantum Mechanical/Molecular Mechanical and Density Functional Theory Studies of a Prototypical Zinc Peptidase (Carboxypeptidase A) Suggest a General Acid-General Base Mechanism. *J. Am. Chem. Soc.* **2009**, *131*, 9780–9788.
- (36) Xu, D.; Guo, H.; Cui, Q. Antibiotic Deactivation by a Dizinc β -Lactamase: Mechanistic Insights from QM/MM and DFT Studies. *J. Am. Chem. Soc.* **2007**, *129*, 10814–10822.
- (37) MacKerell, A. D., Jr.; Bashford, D.; Bellott, M.; Dunbrack, R. L.; Evanseck, J. D.; Field, M. J.; Fischer, S.; Gao, J.; Guo, H.; Ha, S.; Joseph-McCarthy, D.; Kuchnir, L.; Kuczera, K.; Lau, F. T. K.; Mattos, C.; Michnick, S.; Ngo, T.; Nguyen, D. T.; Prodhom, B.; Reiher, W. E., III; Roux, B.; Schlenkrich, M.; Smith, J. C.; Stote, R.; Straub, J.; Watanabe, M.; Wiorkiewicz-Kuczera, J.; Yin, D.; Karplus, M. All-Atom Empirical Potential for Molecular Modeling and Dynamics Studies of Proteins. *J. Phys. Chem. B* **1998**, *102*, 3586–3616.
- (38) Reuter, N.; Dejaegere, A.; Maigret, B.; Karplus, M. Frontier Bonds in QM/MM Methods: A Comparison of Different Approaches. *J. Phys. Chem. A* **2000**, *104*, 1720–1735.
- (39) Shaw, K. E.; Woods, C. J.; Mulholland, A. J. Compatibility of Quantum Chemical Methods and Empirical (MM) Water Models in Quantum Mechanics/Molecular Mechanics Liquid Water Simulations. *J. Phys. Chem. Lett.* **2009**, *1*, 219–223.
- (40) Brooks, C. L., III; Karplus, M. Deformable Stochastic Boundaries in Molecular Dynamics. *J. Chem. Phys.* **1983**, *79*, 6312–6325.
- (41) Ranaghan, K. E.; Ridder, L.; Szefczyk, B.; Sokalski, W. A.; Hermann, J. C.; Mulholland, A. J. Insights into Enzyme Catalysis from QM/MM Modelling: Transition State Stabilization in Chorismate Mutase. *Mol. Phys.* **2003**, *101*, 2695–2714.
- (42) Ryckaert, J.-P.; Ciccotti, G.; Berendsen, H. J. C. Numerical Integration of the Cartesian Equations of Motion of a System with Constraints: Molecular Dynamics of N-Alkanes. *J. Comput. Phys.* **1977**, *23*, 327–341.
- (43) Lodola, A.; Mor, M.; Zurek, J.; Tarzia, G.; Piomelli, D.; Harvey, J. N.; Mulholland, A. J. Conformational Effects in Enzyme Catalysis: Reaction via a High Energy Conformation in Fatty Acid Amide Hydrolase. *Biophys. J.* **2007**, *92*, L20–L22.
- (44) Woodcock, H. L.; Hodoscek, M.; Brooks, B. R. Exploring SCC-DFTB Paths for Mapping QM/MM Reaction Mechanisms. *J. Phys. Chem. A* **2007**, *111*, 5720–5728.
- (45) Kumar, S.; Rosenberg, J. M.; Bouzida, D.; Swendsen, R. H.; Kollman, P. A. The Weighted Histogram Analysis Method for Free-Energy Calculations on Biomolecules. I. The Method. *J. Comput. Chem.* **1992**, *13*, 1011–1021.
- (46) Lonsdale, R.; Hoyle, S.; Grey, D. T.; Ridder, L.; Mulholland, A. J. Determinants of Reactivity and Selectivity in Soluble Epoxide Hydrolase from Quantum Mechanics/Molecular Mechanics Modeling. *Biochemistry* **2012**, *51*, 1774–1786.
- (47) Mujika, J. I.; Lopez, X.; Mulholland, A. J. Mechanism of C-Terminal Intein Cleavage in Protein Splicing from QM/MM Molecular Dynamics Simulations. *Org. Biomol. Chem.* **2012**, *10*, 1207–1218.
- (48) Krokeide, I. M.; Synstad, B.; Gaseidnes, S.; Horn, S. J.; Eijsink, V. G. H.; Sorlie, M. Natural Substrate Assay for Chitinases Using High-Performance Liquid Chromatography: A Comparison with Existing Assays. *Anal. Biochem.* **2007**, *363*, 128–134.